

# Measurement of short-lived particles at PETRA

Autor(en): **Saxon, D.H.**

Objektyp: **Article**

Zeitschrift: **Helvetica Physica Acta**

Band (Jahr): **60 (1987)**

Heft 5-6

PDF erstellt am: **27.04.2024**

Persistenter Link: <https://doi.org/10.5169/seals-115872>

## **Nutzungsbedingungen**

Die ETH-Bibliothek ist Anbieterin der digitalisierten Zeitschriften. Sie besitzt keine Urheberrechte an den Inhalten der Zeitschriften. Die Rechte liegen in der Regel bei den Herausgebern.

Die auf der Plattform e-periodica veröffentlichten Dokumente stehen für nicht-kommerzielle Zwecke in Lehre und Forschung sowie für die private Nutzung frei zur Verfügung. Einzelne Dateien oder Ausdrucke aus diesem Angebot können zusammen mit diesen Nutzungsbedingungen und den korrekten Herkunftsbezeichnungen weitergegeben werden.

Das Veröffentlichen von Bildern in Print- und Online-Publikationen ist nur mit vorheriger Genehmigung der Rechteinhaber erlaubt. Die systematische Speicherung von Teilen des elektronischen Angebots auf anderen Servern bedarf ebenfalls des schriftlichen Einverständnisses der Rechteinhaber.

## **Haftungsausschluss**

Alle Angaben erfolgen ohne Gewähr für Vollständigkeit oder Richtigkeit. Es wird keine Haftung übernommen für Schäden durch die Verwendung von Informationen aus diesem Online-Angebot oder durch das Fehlen von Informationen. Dies gilt auch für Inhalte Dritter, die über dieses Angebot zugänglich sind.

**MEASUREMENT OF SHORT-LIVED PARTICLES AT PETRA**

**D H Saxon**  
**Rutherford Appleton Laboratory**  
**Chilton, Didcot, Oxon, OX11 0QX**

**A B S T R A C T**

The contribution of PETRA to the measurement of short-lived particles is reviewed with discussion of the detectors and analysis techniques. New results are presented on lifetimes of identified particles and the systematics of b-life measurement outlined. The first application of vertex-tagging to flavour separation is described.

**1. INTRODUCTION**

A great attraction of  $e^+e^-$  annihilation is that it is flavour-blind. The creation of fermion species depends only on their charge. Thus  $\tau^+\tau^-$  pairs are created (at  $W = 34$  to  $46$  GeV) equally with  $\mu^+\mu^-$  pairs, and c and b quarks as much as u and d quarks respectively. It provides therefore a special window on to higher generations, and in the case of the third generation particles ( $\tau, b$ ) the only route, so far, to measuring their lifetimes.

The lifetimes involved are small. The  $D^0$  for example, mass  $1.8$  GeV, lifetime  $3 \cdot 10^{-13}$  s, ( $c\tau = 90$   $\mu\text{m}$ ) will travel typically  $800$   $\mu\text{m}$  in the detector before decay, and a b-quark, lifetime  $1 \cdot 10^{-12}$  s, travels  $900$   $\mu\text{m}$ . This sets the scale for the detector required. Synchrotron radiation forces the detector to begin beyond  $5$  cm radius so that an extrapolation is required. The Lorentz boost of the particles ( $\gamma = 3$  to  $7$ ) mean that decay opening angles are small (typically  $200$  mrad), so that transverse errors on particles trajectories below  $100$   $\mu\text{m}$  are needed.

To study short-lived particles, vertex detectors have been installed in three of the detectors, by TASSO in 1982<sup>1,2</sup>, JADE for running in 1985<sup>3</sup>, and in Mark J for running in 1986<sup>4,5</sup>. The TASSO vertex detector has seen  $140$   $\text{pb}^{-1}$  of running at  $35$ - $46$  GeV. To date the 1985 data from JADE have been studied ( $20$   $\text{pb}^{-1}$ ) and results will be obtained from an additional  $100$   $\text{pb}^{-1}$  in 1986. The bulk of the results available to date are therefore from TASSO. First, however, we described the detectors.

**2. VERTEX DETECTORS AT PETRA**

**2.1 JADE.** The JADE vertex detector is illustrated in Figure 1. It is  $760$  mm long and is mounted on an inner beam pipe of  $3$  mm thick Al. The first sense wires are at  $99$  mm radially from the vertex. The chamber consists of  $24$  jet-cells each of  $7$  layers (total  $168$  sense wires), arranged radially, without sense-wire stagger. The sense wires ( $20$   $\mu\text{m}$  W-Re), are maintained at  $+1475$  V ( $+240$  kV/cm) and the potential wires are ground. Graded HV strips at the inner and outer radii ensure a uniform drift field to the HV plane. The maximum drift distance varies from  $13$  to  $20$  mm. It is filled with  $\text{Ar}:\text{CO}_2:\text{CH}_4$  ( $89.1:9.9:1$ ) at  $1.15$  bar and read out with  $100$  MHz FADCs.  $130$  micron  $r$ - $\phi$  resolution has been achieved and  $1.5$  mm double hit resolution. This, together with the seven close points, gives it excellent track-finding properties, and calibration of systematics within one drift cell is presumably straight

forward. It relies on extrapolation from the jet chamber<sup>6</sup> to resolve left-right ambiguities. The chamber first ran in 1985 and physics output from the full 1986 luminosity is expected soon.

**2.2 Mark J.** The Mark J vertex detector was installed for the 1986 running<sup>4,5</sup>. It is an advanced concept offering exciting performance as a time-expansion chamber<sup>7</sup> (see Figure 2). A narrow beam-pipe (5 cm radius) allows the first sense layer to be at 59 mm and 14 layers occur within 45 mm radius. The chamber cells (12 in all) are divided into drift regions and an amplification region. The electric field in the drift region is controlled precisely to allow the use of a non-saturated gas (CO<sub>2</sub>:isobutane - 80:20) at 1.9 bar), with 7  $\mu\text{m}/\text{ns}$  drift. Great care is needed in the control of gas composition and temperature to keep the systematic errors down. With a 100 MHz FADC system  $r\phi$  resolutions of 40  $\mu\text{m}$  have been achieved on Bhabha events and 60  $\mu\text{m}$  on cosmics, with a two-track resolution of 300  $\mu\text{m}$  at 50% efficiency. Unfortunately in running an aging problem occurred, whose origin is not yet clear. Running continued with CO<sub>2</sub>:Ar:ethanol (85:15:3). Vertex detectors for future colliders (LEP, SLC, HERA and beyond<sup>8</sup>) will clearly require the position and two track resolution, and track-finding ability implied by these figures and such a density of points on tracks.

**2.3 TASSO.** The TASSO vertex detector was installed earlier than the others<sup>1,2</sup>. It is of a simpler design, but has now had time to mature its analysis techniques. The layout is shown in Figure 3. Space was found for the insertion of the vertex detector by removal of the beam pipe and replacing it with a smaller diameter thin (0.005 RL) pipe and a system of radiation masks to shield the detector.

This allowed eight sense layers, starting at 81 mm radius in two groups of four. A total of 720 wires provide single-hit readout. The gas used is Ar:CO<sub>2</sub> (95:5), bubbled through ethanol, at 3 bar (38  $\mu\text{m}/\text{ns}$  saturated drift). A constant fraction discriminator system and 0.5 ns TDCs gave precisions of below 100  $\mu\text{m}$  on  $\mu^+\mu^-$  events and 130  $\mu\text{m}$  (including the effect of false assignments) in multi-hadron events. The cells are offset in alternate layers to resolve left-right ambiguity, provide a ready self-calibration, and provide hits in alternate layers on very close tracks. 140 pb<sup>-1</sup> of data were taken between 1982 and 1986 and results are given below. Since the vertex detector is mounted on the beam pipe and not on the drift-chamber, calibration of relative location and Euler angles of alignment was necessary, and movement occurred over running periods.

### 3. VERTEX RECONSTRUCTION TECHNIQUE

Figure 4 shows an event containing a  $D^0 \rightarrow K^-\pi^+$  decay reconstructed in the detector, with a portion of the vertex detector inset. The points associated with the tracks by the track finder are indicated by squares and unassociated hits, including left-right ambiguities, by crosses. Typical measurement resolutions are 220  $\mu\text{m}$  in the drift chamber (outer 9 layers), and 130  $\mu\text{m}$  in the vertex detector. The proportional chamber provides four close points valuable in track-linking and triggering. The stereo layers in the drift chamber are omitted for clarity.

When track-finding in dense jets at high energy, problems can occur. In vertex reconstruction we also reject tracks with fewer than five vertex detector hits. There are additional problems due to the creation of false tracks by stealing points from good ones, and of confusion in extrapolating

In addition one allows for the rejection of points from tracks during fitting. If the  $\chi^2/DF$  exceeds 2 on convergence one makes trial rejections of points and removes that whose elimination causes the greatest reduction. Monte Carlo studies show that an average track of 20 points contains two incorrect assignments, and one of these is readily removed by this procedure.

One then makes constrained vertex fits in a similar way<sup>11</sup>, however not allowing any further point deletion, as one wishes to use the change in  $\chi^2$  on adding vertex constraints as a test of whether tracks truly intersect. The number of constraints  $N_c = \text{No of tracks} - 2$  for two dimensional fits and  $N_c = 2 \times (\text{No of tracks}) - 3$  for three dimensional fits. The result is a reconstructed vertex with quality tests available and a full error matrix on all variables. Typical errors on the flight path of a  $\tau$  (projected on the  $r\phi$  plane) are 1000  $\mu\text{m}$ .

In reconstructing  $D^0$  decays one goes a step further\*. The geometrical fits to  $D^0 \rightarrow K^-\pi^+$  has only one constraint in three dimensions. One gains accuracy in vertex reconstruction by making a kinematic constraint to the  $D^0$  mass (16% error reduction)<sup>14</sup>. Kinematic constraints were also used in the decay  $D_s \rightarrow \phi\pi^+$ ,  $\phi \rightarrow K^+K^-$ , constraining the  $K^+K^-$  to the  $\phi$ -mass, to improve the  $D_s$  signal. A second constraint on the  $D_s$  mass was not imposed as, although it sharpens the errors on true  $D_s$  events, it tends to broaden the distribution for the background when (falsely) constrained to the  $D_s$  mass<sup>15</sup>.

#### 4. THE PRODUCTION POINT

The production point presumably lies within the beam collision envelope, which is about 2.5 cm long along the beam direction. z-measurement quality is worse than  $r\phi$ -reconstruction, and so one always calculates the production point and the flight path only in the  $r\phi$ -plane, and then projects into three dimensions using track momentum directions.

Ideally one would like to reconstruct a production vertex separately for each event. This has been done for b-life studies by MAC<sup>16</sup>, and for b-tagging (Section 7 below) by TASSO. However, it is not without difficulties. It is vulnerable to track finding errors and multiple scattering of slow tracks. One cannot afford to be too choosy as in the case of b-events of the 17 tracks at  $W = 42.1$  GeV, only 5.6 come from the primary vertex. Further, one does not know which ones these are.

Normally one uses the beam spot to estimate the production point. This is unbiased event-by-event and allows many checks of systematics. It is, however, rather large in the horizontal plane owing to the beam energy spread, and this makes a significant contribution to the flight path error. One finds the beam position by accumulating tracks from many events (beam-beam and beam-gas) and looking for the optimal ellipse location to contain points on all tracks. The variation in time in the beam spot centre is indicated in Figure 5(a), which covers four months running. Periods of stability alternate with considerable movement (8 mm range). The y-co-ordinate (not shown) is much more stable as it is less sensitive to storage ring operation conditions. The beam size is then determined by intersecting two prong tracks with the ellipse (see Figure 5(b)). One finds for the beam size  $\sigma_x = 325 \pm 10 \mu\text{m}$  and  $\sigma_y = 86_{-35}^{+20} \mu\text{m}$  at  $W = 34$  GeV<sup>17</sup>. Accelerator calculations are consistent but

\*We shall specify just one charge state in this paper throughout, including by implication also the charge-conjugate state.

close tracks from the drift chamber into the vertex detector<sup>9</sup>. These problems would be reduced in a chamber designed with greater continuity so that the risk of track derailing between drift chamber and vertex detector, or between the inner and outer four layers of the vertex detector, is reduced. Equally, the generation of spurious tracks and the theft by them of points from good tracks, would be suppressed by the more stringent minimum track quality demands that could be made. The performance is considerably better at  $W = 34$  GeV than at  $W = 46$  GeV, since at the lower energy multiplicities are lower, radiation background much reduced, and opening angles are larger.

The steps in reconstructing a secondary vertex are as follows. First, the candidate events and tracks must be found. In the case of  $D^0$ , identified in hadronic events, this means the best possible momentum resolution<sup>10</sup>. A momentum resolution of  $\Delta p_T/p_T = 0.009 p_T$  (GeV) or better is achieved by one of two means - a fit to the found points through the vertex detector and the drift chamber<sup>11</sup>, or a fit to the drift chamber and proportional chamber alone but constraining the tracks to pass through the beam intersection spot. Using an effective spot size of 300  $\mu\text{m}$  radius, this does not introduce significant distortions into charm decays, as the transverse error introduced is small. The relative merit of the two methods, involving different track finders, were studied at length and it was established that the same event samples were obtained<sup>9,10</sup>.

The tracks wanted in the secondary vertex must be found and reconstructed. As indicated above, two different track finders were used. One extrapolated tracks found in the drift chamber and proportional chamber into the vertex detector, and the other treated all devices equally ab initio<sup>12,13</sup>. In crowded events they had complementary virtues and vices. In order to have a stable simulation, readily simulated by Monte Carlo, it was decided in each case to use one of the finders for physics analysis, and the other as a check. The accuracy of the Monte Carlo simulation is sensitive to the assumed input of random and correlated noise in the vertex detector, particularly at  $W = 44$  GeV.

For accurate reconstruction of tracks one requires a formalism which is exact for points lying on the true trajectory. One wishes to be sensitive to displacements of 10  $\mu\text{m}$  over a track of length 1 m and radius 10 m and to avoid numerical rounding errors in calculation. For a track passing at distance  $d_0$  from the origin in the  $(x, y)$  plane at azimuthal angle  $\phi_0$  with radius  $r_0$  and (charge  $\times$  sign of magnetic field)  $Q$ , TASSO use the form<sup>11</sup>:

$$d(x, y) = \frac{1}{2}K(x^2 + y^2 - d_0^2) + x\sin\phi_0 - y\cos\phi_0 + d_0Q - \epsilon$$

$$\text{where } K = -Q/(r_0 - d_0)$$

One can verify that  $d = 0$  for points on a circle. This form is easily extended to allow for stereo layers. The term  $\epsilon = 0$  for  $r < a$  ( $r^2 = x^2 + y^2$ ), and  $\epsilon = \theta(r - a)$  for larger radii. This term represents multiple scattering in the material between the VXD and DC, represented as a single layer of 0.075 RL. Introducing a

$$\chi^2 = \sum_1 d_i^2/e_i^2 + \theta^2/\theta_0^2,$$

where the sum runs over the measured points, one has a formalism in which error matrices on track and vertex quantities can be calculated and used in subsequent fits.

suggest a rather smaller vertical dimension<sup>18</sup>. At  $W = 44$  GeV, the horizontal dimension grows to about  $420 \mu\text{m}$ .

Knowing the beam centre and size, and the reconstructed decay vertex and error and the flight path direction, one can reconstruct the production point as the best intersection of the flight path and beam ellipse. One finds for the three-dimensional flight path:

$$l = \frac{x_v \sigma_{yy} t_x + y_v \sigma_{xx} t_y - \sigma_{xy} (x_v t_y + y_v t_x)}{\sigma_{yy} t_x^2 - 2\sigma_{xy} t_x t_y + \sigma_{xx} t_y^2}$$

where  $(x_v, y_v)$  is the distance from beam spot centre to decay vertex,  $\sigma$  is the error matrix on this (obtained by adding elements of the production and decay error matrices) and  $t_x, t_y$  are direction cosines of the flight path ( $t_x^2 + t_y^2 + t_z^2 = 1$ ).

## 5. LIFETIME MEASUREMENTS OF IDENTIFIED PARTICLES

5.1  $\tau$ -Lepton. Measurement of the  $\tau$  lifetime tests  $\tau, \mu$  universality. If the strength of the  $(\tau\nu_\tau W)$  vertex is equal to that of the  $(\mu\nu_\mu W)$  vertex then the two lifetimes are related by:

$$\tau(\tau) = \tau(\mu) \left( \frac{m_\mu}{m_\tau} \right)^5 \text{BR}(\tau \rightarrow e\nu)$$

The branching ratio  $\tau \rightarrow e\nu$  enters because the  $\tau$  has hadronic decay channels, not open in  $\mu$ -decay, and not exactly calculable. From results by the Mark II and TPC experiments one obtains  $\text{BR}(\tau \rightarrow e\nu) = (17.9 \pm 0.4)\%$ <sup>19</sup>. This yields a prediction of:

$$\tau(\tau) = (2.86 \pm 0.07) 10^{-13} \text{ s}$$

The  $\tau$ -decay point is reconstructed from the  $\tau \rightarrow 3$  prong decay mode (BR  $13.1 \pm 0.3\%$ ), and the production point from the beam spot. One can additionally make a measurement from the separation of decay points when both  $\tau$ 's in  $e^+e^- \rightarrow \tau^+\tau^-$  decay to three charged particles. This has two advantages - it does not need knowledge of the production point, and the most probable separation is not zero (in contrast to the most probable decay length). However, the statistic is low, so it is used only as a check.

Figure 6(a) shows preliminary results based on all data taken at PETRA by TASSO. This updates an earlier publication<sup>2</sup>. The curve represents the predicted distribution from a maximum likelihood fit, using the event-by-event error distribution shown in Figure 6(b). One obtains:

$$\tau(\tau) = (2.89 \pm .21 \pm .15) 10^{-13} \text{ s} \quad \text{TASSO prelim}$$

This is compared to other measurements in Table 1, where statistical and systematic errors have been added in quadrature<sup>20</sup>.

$\tau, \mu$  universality is clearly verified to  $\pm 5\%$ . Further improvement in lifetime measurements is justified in view of the high accuracy of branching ratio measurements;  $\pm 3.5\%$  should be attainable.

5.2 Charmed Mesons. Based on a spectator model (Figure 7(a)) one expects:

$$\tau(D^+) \geq \tau(D^0) = \tau(D^S) = \frac{1}{5} \left( \frac{m_\mu}{m_c} \right)^5 \tau_\mu$$

**T A B L E 1**  
**τ-LIFETIME SUMMARY**

Expt	Result	Reference
TASSO	$(2.89 \pm 0.26) 10^{-13} \text{ s}$	Preliminary
Mark II	$(2.86 \pm 0.30) 10^{-13} \text{ s}$	21,22
MAC	$(2.84 \pm 0.21) 10^{-13} \text{ s}$	20,23
CLEO	$(3.15 \pm 0.34) 10^{-13} \text{ s}$	20
HRS	$(2.80 \pm 0.30) 10^{-13} \text{ s}$	20
<b>Average</b>	<b><math>(2.89 \pm 0.12) 10^{-13} \text{ s}</math></b>	

where the  $D^+$  life can be lengthened because of destructive interference between the two  $\bar{d}$  quarks. Note that the Cabibbo angle does not enter here as one sums over  $Q' = s$  and  $d$ . However, other diagrams can also contribute. The annihilation diagram (Figure 7(b)) contributes for  $D_s$  and the exchange diagram for  $D^0$ . The contribution of the annihilation diagram is not expected to be influential as it is angular-momentum suppressed without additional gluons, but the exchange diagram can shorten the  $D^0$  life. One therefore expects that the  $D^0$  life may be significantly less than the  $D^+$  life. A complete theory should explain all three lifetimes. Penguin diagrams (Figure 7(d)) contribute to certain final states (eg  $D^0 \rightarrow \phi K^0$ ) but have little influence on the overall rate. (See Reference 20 and references therein.)

TASSO have published a  $D^0$ -life measurement based on fifteen events taken up to the end of 1985<sup>10</sup>. Including the 1986 data from the channels  $D^{*+} \rightarrow D^0\pi^+$ ,  $D^0 \rightarrow K^-\pi^+$  and  $K^-\pi^+(\pi^0 \text{ unse})$  gives a total of 60 events. The mass difference  $\Delta m = m(D^*) - m(D)$  plots for these channels are given in Figure 8(a,b) and the decay length distribution in Figure 8(c). Figure 8(d) shows the decay time distribution for a control sample in the  $D^0$  upper side-band. Allowing for 4.5%  $b$  contamination one obtains for the control  $\tau = (0.06 \pm 0.2) 10^{-13} \text{ s}$  where 0 is expected, and from the width of the distribution a scale factor  $(1.04 \pm 0.05)$  on the errors. The fit to the data then yields:

$$\tau(D^0) = (4.8_{-0.9}^{+1.0} \pm 0.8) 10^{-13} \text{ s} \quad \text{TASSO prelim}$$

A particular problem of loss of data occurs in the  $D^0$  lifetime measurement since the  $Q$ -value for the decay  $D^{*+} \rightarrow D^0\pi$  is so low. Looked at in projection the transition pion is almost always close to one or other of the decay tracks of the  $D^0$ . This can result in a loss of points from these tracks and confusion in track-finding. Care must be taken to ensure a sample of clean data without errors, and to treat Monte Carlo similarly. Roughly half the  $D^0$  candidates survive linkage into the vertex detector and quality cuts. Similar losses, though less severe, occur in reconstruction of  $D_s \rightarrow \phi\pi^+$ ,  $\phi \rightarrow K^+K^-$ .

The  $\phi\pi^+$  mass spectrum for  $x > 0.6$  is shown in Figure 9(a) after applying  $\phi$  mass constraint and  $\chi^2$  cut to  $K^+K^-$  combinations. A signal of 9 events is seen over a background of 5, corresponding to a Branching ratio for  $D_s \rightarrow \phi\pi^+$  of  $(3.3 \pm 1.6 \pm 1.0)\%$ , close to the values seen in other experiments<sup>24</sup>. The decay time distribution is shown in Figure 9(b). This gives a value:

$$\tau(D_s) = (5.7_{-2.6}^{+3.6} \pm 0.9) 10^{-13} \text{ s} \quad \text{TASSO}^{15}.$$

Allowance is made for charm contaminations of 7%  $D^0$ , 8%  $D^+$  and negligible  $\Lambda_c$ . As a quality check, a control sample was set up using  $1.05 < m(KK) < 1.15$  and  $2.02 < m(KK\pi) < 2.50$  GeV (17%  $D^0$ , 17%  $D^+$ ). The decay time distribution for this sample is shown in Figure 9(c) together with the prediction. The close agreement of prediction and experiment verifies the background estimation, resolution calculation and lack of bias. If a light-quark lifetime is extracted one obtains  $\tau(\text{ud}) = (-.59 \pm .43) 10^{-13}$  s, consistent with no bias.

The  $D^0$ -life measurement is compared to other results from storage rings in Table 2, and to selected fixed target results. The fixed target results are more incisive, as also for the  $D^+$  and  $D_s$  where one obtains:

$$\tau(D^+) = (10.4 \pm 0.4) 10^{-13} \text{ s} \quad [\text{From References 20,28}]$$

$$\tau(D_s) = (3.5_{-0.5}^{+0.6}) 10^{-13} \text{ s}^{20}$$

$$\text{and } \tau(D^+)/\tau(D^0) = 2.40 \pm 0.05$$

We conclude that the difference between the  $D^+$  and  $D^0$  lifetimes is clearly established, though not yet the mechanism. The future of charm lifetime measurements seems to lie in fixed-target work. The third generation ( $\tau$ ,  $b$ ) remains the province of  $e^+e^-$  storage rings.

## 6. MEASUREMENT OF THE b-LIFE

6.1 Methodology.  $b$ -decay involves a transition between generations, and its rate is therefore governed by quark-mixing elements of the Kobayashi-Maskawa matrix. For maximal mixing one expects a lifetime of order  $10^{-15}$  s. Based on a semi-leptonic branching ratio of  $(11.8 \pm 0.3 \pm 0.6)\%$  one obtains:

$$\tau(b) = [4.9 |V_{cb}|^2 + 10.0 |V_{ub}|^2]^{-1} 10^{-14} \text{ s}^{29}$$

There is no evidence for  $b \rightarrow u$  transitions. We shall therefore interpret the result in terms of a measurement of  $|V_{cb}|^{20}$ . Measureable lifetimes can arise only through strong suppression of generation mixing.

A lifetime of  $10^{-12}$  s gives rise to a typical decay length of 900  $\mu\text{m}$ . The statistics are now adequate and the accuracy is limited by systematics. For this reason the 1986 results, which will greatly increase the statistic, and include the first results from the JADE vertex detector, are not yet available, as time and care are required in systematic error reduction. We discuss here the methods used so far, and the results obtained on earlier data.

$b$ -events comprise 9% of the total  $e^+e^- \rightarrow \text{hadrons}$  events.  $b$ -decay therefore influences the vertex quality of the average event. One may well wish, however, to select  $b$ -events using either the event shape to tag the high  $b$ -quark mass, or inclusive high  $p_T$  leptons as a signature.

**TABLE 2**  
**D<sup>0</sup>-LIFETIME SUMMARY**

Expt	Result	Reference
<u>e<sup>+</sup>e<sup>-</sup> Storage Rings</u>		
TASSO	$(4.8 \pm 1.3) 10^{-13} \text{ s}$	Preliminary
HRS	$(4.2 \pm 1.1) 10^{-13} \text{ s}$	20
CLEO	$(5.0 \pm 0.8) 10^{-13} \text{ s}$	20
Mark II	$(4.2 \pm 2.1) 10^{-13} \text{ s}$	25
DELCO	$(4.6 \pm 1.7) 10^{-13} \text{ s}$	26
<u>Fixed Target</u>		
ACCMOR	$(3.9_{-0.5}^{+0.6}) 10^{-13} \text{ s}$	20
LEBC	$(4.2_{-0.4}^{+0.5}) 10^{-13} \text{ s}$	20
E531	$(4.3_{-0.5}^{+0.7}) 10^{-13} \text{ s}$	27
E691	$(4.35 \pm 0.18) 10^{-13} \text{ s}$	28
<b>World Average</b>	<b><math>(4.33 \pm 0.13) 10^{-13} \text{ s}</math></b>	

In a b-event the multiplicity is typically 17.2 charged tracks ( $W = 42.1 \text{ GeV}$ ). 11.5 of these come from b-decay or from subsequent charm decay and 5.7 from the production vertex. Selecting high  $p_T$  leptons picks tracks preferentially from the b-decay. Methods using hadronic tracks must take account of the 5-vertex structure of an event (see Figure 10(a)).

For the production point one normally uses the beam spot. MAC have recently published a result using a vertex established event-by-event<sup>17</sup>.

Finally, one should face the question, which B-meson is one observing,  $B^0$ ,  $B^-$ ,  $B_c$ ,  $B_s$ ? If spectator decays dominate and all have the same branching ratios it does not matter. There is only one unbiased B-meson decay in flight event established (in emulsion)<sup>30\*</sup>. We have to resort to averaging. Hadronic selection weights  $B^0$ ,  $B^+$  according to production rates (perhaps equal, with  $B_s$  suppressed?). Leptonic selection preferentially picks to the meson of longer decay time. From the study of dilepton events CLEO have found  $0.44 < \tau(B^0)/\tau(B^+) < 2.05$ <sup>31</sup>.

In measuring b-lifetimes, most methods make use of the "impact parameter" defined as the amount by which a track, extrapolated back, misses the production point in the  $r\phi$  projection (see Figure 10(b)). The decay length in the laboratory is typically  $\beta\gamma c\tau$ , and the opening angle of the decay

\*The short-lived decay in this event was part of the trigger. A significantly longer decay time would have caused loss of the event.

$a \sim \gamma^{-1}$ . The impact parameter is therefore  $\delta \sim c\tau/f$  where  $f \sim 2$ . Thus  $\delta \sim 150 \mu\text{m}$  for  $\tau = 1 \text{ ps}$ . If the b-flight direction is known, one can assign a sign to  $\delta$ . A positive  $\delta$  corresponds to a positive decay time and negative otherwise. This arises through measuring errors and scattering. One does not know the b-direction and so uses the jet (sphericity) axis as an estimator. Monte Carlo studies indicate errors of order 100 mrad in this technique.

The great advantage of impact parameter studies of lifetime is that one needs to know neither the decay vertex nor the energy of the b-particle, only that it was fast, as expected for heavy quark fragmentation<sup>32</sup>. Thus no reconstruction of B particles is needed. For the average hadronic event (uds:c:b) = 6:4:1, one finds<sup>33</sup>  $\langle \delta \rangle = 20 \mu\text{m} + 0.07 c\tau_c + 0.04 c\tau_b$ .

The first term arises from undetected  $K^0$ ,  $\Lambda^0$  decays and  $\gamma$ -conversion, the second from charm decays (average multiplicity 4.6 secondaries/event) and the last from b-decays (11.5 secondaries/event).

We now look in turn at four methods of measuring  $\tau(b)$ , two based on event selection and impact parameter, and two involving decay vertices and complete event samples. A strong motivation for this multi-pronged approach is the independence of the systematic errors.

**6.2 Event Shape Selection.** In this method, TASSO use the large Q value of B-meson decay as an event signature<sup>33</sup>. The event should have two fat hemispheres (in contrast to a  $q\bar{q}g$  event with one fat and one thin jet). The method is to find the sphericity axis, cut the event in half, boost each jet by  $\beta = 0.7$  towards its centre of mass and calculate the sphericity of each jet,  $S_1$  and  $S_2$ . If  $S_1 S_2 > 0.1$  we accept the event as b-enriched (14% pass rate, 32% b). If  $S_1 S_2 < 0.04$  we define it as b-depleted. For the b-enriched sample for tracks of  $p > 1 \text{ GeV}/c$  (uds:c:b  $\sim$  1:1:1)  $\langle \delta \rangle = 30 \mu\text{m} + 0.07 c\tau_c + 0.14 c\tau_b$  approximately. Based on  $25 \text{ pb}^{-1}$  of data with the vertex detector one finds  $\langle \delta \rangle = 91 \pm 17 \mu\text{m}$  for the b-enriched sample and  $38 \pm 8 \mu\text{m}$  for the b-depleted sample (see Figure 11). From comparison with Monte Carlo one finds

$$\tau(b) = 1.57 \pm 0.32_{-0.34}^{+0.37} \text{ ps}^{29,34}$$

The main systematic error arises in the uncertainty in b-enrichment.

**6.3 Lepton Tag Selection.** The JADE group have measured the b-life by this means<sup>35</sup>, and were the first group to attempt measuring b-lifetimes in  $e^+e^-$  annihilation<sup>36</sup>. All of the data used are without the vertex detector. The impact parameter method is sufficiently immune to systematics that averaging over a sample with large individual errors is quite acceptable. They select b-events by looking for a muon of  $p_T > 0.9 \text{ GeV}/c$  wrt the sphericity axis, isolated from other tracks in an event of significant acoplanarity (to suppress  $q\bar{q}g$  events) 74 muon candidates survive, estimated as 65%  $b \rightarrow \mu$ , 6%  $b \rightarrow c \rightarrow \mu$ , 8%  $c \rightarrow \mu$  and 21% misidentified hadrons. Similarly an electron-tagged sample (25 events) is found, estimated as 80%  $b \rightarrow e$ , 8%  $b \rightarrow c \rightarrow e$ , 10%  $c \rightarrow e$  and  $< 3\%$  fake. The mean impact parameters of these lepton tracks are  $282 \pm 78 \mu\text{m}$  and  $457 \pm 107 \mu\text{m}$  respectively (see Figure 12), from which one calculates

$$\tau(b) = (1.76_{-0.38}^{+0.45} \pm .38) \text{ ps}^{35}$$

Note that by selecting events with a lepton tag, and then using the lepton impact parameter, one preferentially selects the B-meson with longer lifetime, given that the semileptonic widths are equal. The systematic errors are dominated by the uncertainty in the b-fraction, including the uncertainty on the  $b \rightarrow \mu, e$  branching ratios.

JADE have also investigated a method which weights events with a probability for being a b, based on the event aplanarity and  $p_T$  of the muon with respect to the jet. All 293 inclusive muon events can be used. They compare weighted and unweighted samples and extrapolate to pure b and pure background. They do this both for muon tracks and for all tracks. (In the second case in the opposite jet there is no bias between  $B^\pm$  and  $B^0$ .) They find  $\tau(B) = 1.7 \pm 0.6 \pm 0.4$  ps, and use this as a check on the validity of the lepton-selection method.

**6.4 Secondary Vertex Reconstruction.** TASSO investigated methods not requiring a b-enrichment of the sample<sup>20,29,37</sup>. For the production vertex they take the event spot and for the b-direction the sphericity axis. All tracks are taken with momentum above 0.6 GeV/c,  $\geq 5$  vertex detector hits, and good  $\chi^2$  ( $\sim 5$  tracks/event). The event is divided in half and all three-track, singly charged, one-jet vertices reconstructed. The vertex with the lowest increase in  $\chi^2$  on adding the vertex constraint is taken as a decay vertex and the two dimensional length histogrammed (Figure 13). An average  $\langle l_{2D} \rangle = 141 \pm 16$   $\mu\text{m}$  is found. From Monte Carlo estimates one subtracts 12  $\mu\text{m}$  for uds-events and 51  $\mu\text{m}$  for charm-events. This leaves 88  $\mu\text{m}$  as the contribution from beauty-events (11.7% of the events used). Monte Carlo calculations are used to relate  $\langle z_b \rangle$ , the mean fractional b-energy, and  $\tau_b$  to  $\langle l_{2D} \rangle$ . They obtain

$$\tau(b) = (1.50_{-.29}^{+.37} \pm .28) \text{ ps}$$

The systematic errors are quite different in origin from those in impact parameter methods:

Assumed detector resolution	$\pm 0.15$ ps
b-fragmentation	$\pm 0.14$ ps
Simulation of track finding	$\pm 0.11$ ps
$N_{ch}$ b-decay	$\pm 0.11$ ps
c-fragmentation	$\pm 0.06$ ps
Charm lifetimes	$\pm 0.06$ ps
Detector misalignment	$\pm 0.05$ ps
Procedure relating $l_{2D}$ to $\tau(b)$	$\pm 0.05$ ps
Light-quark fragmentation	$\pm 0.03$ ps
Beam spot size	<u>0.00 ps</u>
	<u><math>\pm 0.28</math> ps</u>

**6.5 Dipole Method.** This is a second method involving the vertices of an average event, used by TASSO<sup>20,29,37</sup>. In events of sphericity  $< 0.3$  all tracks of momentum above 0.2 GeV/c are used, after cuts to exclude  $K^0$ ,  $\Lambda$  decay. Production point information is not used, analogous to the study of  $\tau^+\tau^- \rightarrow 3 + 3$  prongs.

The method is illustrated in Figure 14. The sphericity axis is moved parallel to itself to make the best intersection with the event tracks. A "production vertex" for each track is found by intersecting the tracks with this axis in the  $r\phi$  projection. An average vertex point is found in each jet

by weighting each track intersection with a weight  $W \sim y \cdot \sin^2 \alpha / \sigma^2$  where the impact parameter error on the track (including multiple scattering) is  $\sigma$ , the angle to the jet axis is  $\alpha$  and the rapidity wrt the jet axis is  $y$ . This last factor is introduced to reduce the sensitivity to b-fragmentation. The best vertex is found for each jet and the event dipole moment,  $\rho = |\langle r \rangle(\text{jet 1}) - \langle r \rangle(\text{jet 2})|$ . Like the average impact parameter of events this method is sensitive to the b-life because of the large Q-values and high multiplicity in b-decay.

The results are shown in Figure 15, compared to Monte Carlo for  $\tau(b) = 1.4$  and 0 ps. The zero-life Monte Carlo is clearly excluded, and one obtains

$$\tau(b) = (1.62_{-.29}^{+.33} \pm .25) \text{ ps}$$

The systematic errors origin is similar to that of the secondary vertex method, except that there is less sensitivity to b-fragmentation

Detector simulation	$\pm 0.15 \text{ ps}$
Different Monte Carlo generators	$\pm 0.11 \text{ ps}$
Charm lifetimes	$\pm 0.10 \text{ ps}$
$K^0, \Lambda$ fraction	$\pm 0.06 \text{ ps}$
$N_{ch}$ b-decay	$\pm 0.05 \text{ ps}$
b-fragmentation	$< 0.06 \text{ ps}$
c-fragmentation	$< 0.06 \text{ ps}$
	<u><math>\pm 0.25 \text{ ps}</math></u>

**6.6 Summary.** b-life results from PETRA and elsewhere are summarised in Table 3. One should beware of averaging, either within or between experiments due to overlap in data sets and in analysis assumptions which couple the random and systematic errors respectively. We make the following observations:

- Any systematic difference between PEP and PETRA is less than  $1.7 \sigma$  (less than this if errors are not independent).
- The 1986 data will reduce the errors on PETRA data, and will include results from the JADE vertex detector.
- $\tau(B^-)/\tau(B^0)$  is consistent with 1. If this were not so  $R = \tau(\text{All b-events})/\tau(\text{lepton-selected})$  would be less than 1. The experimental value is  $R = 1.45_{-.42}^{+.45}$ . For comparison the CLEO dilepton measurements give  $R = 0.99 \pm 0.11^{31}$ . At the present level of accuracy we are therefore not sensitive to any expected differences in the lifetime.
- Taking the errors at face value as independent, we obtain  $\tau(b) = (1.24 \pm 0.11) \text{ ps}$ . If we ignore  $b \rightarrow u$  transitions, this sets  $|V_{cb}| = 0.042 \pm 0.003 \pm 0.005$ , where the first error is experimental and the second theoretical (see Reference 29 for discussion, see also Reference 20). This represents a massive suppression of generation mixing.
- $e^+e^-$  annihilations have provided the only, and accurate, measurements of third-generation fermion lifetimes.

## 7. TAGGING b-EVENTS BY DECAY VERTEX

Vertex detectors at future accelerators will not be employed to repeat the lifetime measurements described above. The emphasis will shift,

**TABLE 3****b-LIFE SUMMARY**  
(See Also Reference 29)

Method	Result (ps)	Reference
<u>All b-decays, TASSO</u>		
S-tag, $\delta$ -hadronic	$1.57 \pm .32^{+.37}_{-.34}$	34
Secondary vertex, all events	$1.50^{+.37}_{-.29} \pm .28$	37
Dipole, all events	$1.62^{+.33}_{-.29} \pm .25$	37
<u>Lepton tag, <math>\delta</math>-leptons</u>		
JADE	$1.76^{+.45}_{-.38} \pm .38$	35
DELCO	$1.16 \pm .16 \pm .17$	20
Mark II	$0.85 \pm .17 \pm .21$	38
HRS	$1.02^{+.41}_{-.37}$	39
<u>Lepton tag, all b-decays</u>		
MAC	$(1.29 \pm 0.20 \pm .07) \pm 15\%$	40
<b>Naive Average</b>	<b><math>1.24 \pm .11</math></b>	

amongst presently known particles, to using vertex properties to tag flavours at production (see for example References 8,41,42). We present here the first such technique used for this in  $e^+e^-$  annihilation, using the TASSO vertex detector information to tag b-events<sup>17</sup>. An event is shown in Figure 16(a), with the vertex region greatly enlarged in Figure 16(b).

First one finds an event vertex. The beam spot provides an accurate enough y-measurement. The x-co-ordinate is improved by intersecting all the tracks with the line  $y = y(\text{spot})$ . Then pairs of tracks are combined to make secondary vertices and, depending on the position and error, assigned a weight  $W = 0$ , if entirely consistent with the production vertex and  $W = 1$ , if inconsistent with this but downstream. The weights of all pairs are added and a cut made on the sum (typically at  $\Sigma W = 4$ ). This can be done either on the whole event, or on a single jet, in which case the recoil jet can be studied in an unbiased way.

The effectiveness of the method depends on the b-lifetime. Taking the world-average one finds in jet-mode tagging a b-purity of 65% with a yield of 33% of all b-events.

Opposite jet properties studied include rapidity, inclusive momentum spectrum,  $p_T^2$  and sphericity, and the strength of the  $b\bar{b}g$  coupling compared to the average  $q\bar{q}g$  coupling. We describe here one application - the determination of the jet charged multiplicity.

Average jets contain uds:c:b in the ratio 55:36:9, and tagged jets 17:22:61. In Figure 17 the jet charged multiplicity distributions of tagged and average jets are compared (a) as measured (b) after correction for detector acceptance, at  $W = 42.1$  GeV. From these results one obtains for jets (= half events)

$$\begin{aligned} \langle N_{\text{ch}} \rangle &= 7.44 \pm 0.03 \pm 0.19 && \text{(average jet)} \\ &8.09 \pm 0.29 \pm 0.16 && \text{(b-enriched)} \\ \text{and hence} &8.51 \pm 0.50 \pm 0.35 && \text{(b-jet)} \end{aligned}$$

by extrapolation. The systematic error on the b-jet multiplicity includes  $\pm 0.27$  for a variation of  $\pm 10\%$  in b-tag purity.

Using the value for b-decay charged multiplicity,  $N_{\text{ch}} = 5.50 \pm 0.16^{43}$ , one obtains the number of associated charged tracks at production, per jet,  $N_{\text{ch}} = 3.3$ .

## 8. CONCLUSIONS

Substantial data samples have been taken at PETRA using precision vertex detectors. Preliminary results based on the full statistic are available for exclusive channels.

The  $\tau$ -life is measured by TASSO as  $\tau(\tau) = (2.89 \pm 0.21 \pm 0.15) 10^{-13}$  s (prelim). Theory predicts  $(2.86 \pm 0.07) 10^{-13}$  s.

The  $D^0$  and  $D_s$  lives have been measured by TASSO. Fixed target measurements are now more accurate for second-generation flavours.

The b-life has been measured by many methods with different systematic errors and event selection, particularly by TASSO. Since systematics dominate, the 1986 results will be shown after careful analysis, but the improved statistic will reduce the errors. Data from the JADE vertex detector will be available. An average of measurements gives

$$\tau(b) = (1.24 \pm 0.11) \text{ ps}$$

There is no evidence for  $\tau(B^-) \neq \tau(B^0)$ . b-decay is strongly suppressed. Setting  $V_{ub} = 0$  one obtains  $|V_{cb}| = 0.042 \pm 0.003 \pm 0.005$ .

The first application of vertex tagging to select b-events has been shown. Detectors at LEP, SLC and elsewhere should follow similar techniques.

PETRA has made a dominant contribution to the study of third-generation lifetimes, particularly in the systematics of b-decay analysis, and opened the way to flavour tagging using vertex information.

## ACKNOWLEDGEMENTS

This report contains a distillation of over five years' experience on hardware and analysis techniques. The DESY directorate have throughout provided a stimulating environment for this work, and the funding agencies of many countries have supported us. On behalf of us all, thank you.

## REFERENCES

1. D M Binnie et al, Nucl Instr Meth **228** (1985) 267.
2. TASSO Collaboration, M Althoff et al, Phys Lett **141B** (1984) 264.
3. C Kleinwort, private communication.

4. H Anderhub et al, Nucl Instr Meth **A252** (1986) 357 and UGVA-DPNC 1987/02-117, presented by M Bourquin at Workshop on Vertex Detectors, Erice 21-26 September 1986.
5. G Viertel, Proc Conf on Adv in Instr for Colliding Beam Experiments, SLAC 9-13 March 1987.
6. H Drumm et al, Nucl Instr Meth **176** (1980) 175.
7. A H Walenta, IEEE Trans Nucl Sci **NS-26** (1) (1978) 73.
8. D H Saxon, RAL-87-011, to be published in Proc Workshop on Physics at Future Accelerators, La Thuile, 7-10 January 1987.
9. D Strom, Thesis, University of Wisconsin (1986).
10. TASSO Collaboration, M Althoff et al, Z Phys **C32** (1986) 343
11. D H Saxon, Nucl Instr Meth **A234** (1985) 258.
12. A Campbell, Thesis, Imperial College London HEP T 117 (1983).
13. W Schütte, Thesis, University of Hamburg, DESY Interner Bericht F1-84/03.
14. G E Forden and D H Saxon, Nucl Instr Meth **A248** (1986) 439.
15. TASSO Collaboration, W Braunschweig et al, DESY 86-159 (1986).
16. W W Ash et al, Phys Rev Lett **58** (1987) 640.
17. D Su, private communication.
18. M Leneke, private communication.
19. P R Burchat, Santa Cruz Report SCIPP 86/72, to be published in Proc 23 Int Conf on HE Phys, Berkeley, 16-23 July 1986.
20. M G D Gilchriese, Cornell Report CLNS 86/754, to be published in Proc 23 Int Conf on HE Phys, Berkeley, 16-23 July 1986.
21. J Jaros, SLAC-PUB-3569 (1984).
22. J Jaros et al, Phys Rev Lett **51** (1983) 955.
23. E Fernandez et al, Phys Rev Lett **54** (1985) 1624.
24. HRS Collaboration, M Derrick et al, Phys Rev Lett **54** (1985) 2568.
25. J M Yelton et al, Phys Rev Lett **52** (1984) 2019.
26. DELCO Collaboration, H Yamamoto et al, Phys Rev **D32** (1985) 2901.
27. N Ushida et al, Phys Rev Lett **56** (1986) 1771.
28. J C Anjos et al, Phys Rev Lett **58** (1987) 311.
29. V Lüth, Invited Talk Presented at Int Symp on Prod and Decay of Heavy Flavours, Heidelberg, 19-23 May 1986. SLAC-PUB-4052 (1986).
30. W Albanese et al, Phys Lett **158B** (1985) 186.
31. A Bean et al, Phys Rev Lett **58** (1987) 183.
32. J Izen, Proc XV Int Symp on Multiparticle Dynamics, Lund 1984 (Ed G Gustafson and C Peterson - World Scientific), 727.
33. TASSO Collaboration, M Althoff et al, Phys Lett **149B** (1984) 524.
34. TASSO Collaboration, Contributed Paper to EPS Meeting, Bari, 1985.
35. JADE Collaboration, W Bartel et al, Z Phys **C31** (1986) 349.
36. JADE Collaboration, W Bartel et al, Phys Lett **114B** (1982) 71.
37. TASSO Collaboration, Contributed paper to 23 Int Conf on HE Phys, Berkeley, 1986.
38. J Jaros, Proc Phys In Collision **4** (1984) 257.
39. D Blockus et al, Argonne Report ANL-HEP-PR-86-144 (1986).
40. W W Ash et al, Phys Rev Lett **58** (1987) 640.
41. C J S Damerell, Rutherford Report, RAL-86-077 (1986).
42. D P Kelsey and M Pepè, Proc Workshop on Physics at Future Accelerators, La Thuile, 7-10 January 1987 (to be published), G Bellettini and G Chiarelli, *ibid*.
43. R Giles et al, Phys Rev **D30** (1984) 2279.

**FIGURE CAPTIONS**

1. The JADE vertex detector (a) cross-section (b) voltages and equipotentials in a drift cell of 7 sense wires.
2. The MARK-J vertex detector (a) cross-section (b) voltages and equipotentials in a drift cell. Fourteen sense wires occur in two groups of seven.
3. (a) View of the central portion of the TASSO detector, viewed perpendicular to the direction of the colliding beams (b) the central portion of the TASSO detector viewed along the direction of the colliding beams (c) an expanded view of part of the aluminium end flange of the detector.
4. An event with  $D^0$  decay reconstructed in the TASSO detector. The tracks marked correspond to the decay  $D^{*+} \rightarrow D^0 \pi^{\pm}$ ,  $D^0 \rightarrow K^- \pi^+$ . (This event has  $m(K^- \pi^+) = 1.869$  GeV and  $\Delta m = 0.145$  GeV.)
5. (a) x-co-ordinate of the beam centre (cm) as a function of run number over a four month period (b) beam size as measured by the impact parameter of two prong tracks.
6. (a) Distribution of  $\tau$  measured decay times, shown as  $c\tau$  in tau rest frame, from 583 reconstructed decays (TASSO). Curve shows prediction resulting from maximum likelihood fit. (b) Distribution of errors on  $c\tau$ .
7. Decay modes of mesons containing heavy quarks. (a) Spectator (b) annihilation (c) exchange (d) penguin, from Reference 20.
8. Mass difference spectrum for  $m(K^- \pi^+ \pi^+) - m(K^- \pi^+)$  from TASSO, demanding  $\geq 4$  VXD hits on each track and good vertex fit quality for events with  $E(K^- \pi^+ \pi^+)/E(\text{beam}) > 0.5$  (a)  $p > 0.8$  GeV/c for  $K^-$  and  $\pi^+$  making  $1.715 < m(K^- \pi^+) < 2.015$  GeV with good kinematic fit to  $D^0$  (b)  $p > 1.4$  GeV/c for  $K^-$  and  $\pi^+$  making  $1.5 < m(K^- \pi^+) < 1.715$  GeV (so called "S<sup>0</sup>" mode corresponding to  $D^0 \rightarrow K^- \pi^+ (\pi^0 \text{ unseen})$ ). Shaded histogram - Monte Carlo background. The region  $\Delta m < 0.150$  GeV is taken as the  $D^0$  region. (c) Decay length spectrum: curve is result of maximum likelihood fit. (d) Control sample.
9. (a)  $\phi \pi^{\pm}$  mass spectrum ( $x > 0.6$ ) for  $K^+ K^-$  constrained to  $\phi$ -mass (TASSO). The  $D_s$  signal is indicated together with the expected  $D^+ \rightarrow \phi \pi^+$  signal. (b) Decay time distribution for  $D_s$  region; curve - result of likelihood fit. (c) Control region (17%  $D^0$ , 17%  $D^+$ ); curve - prediction.
10. (a) Schematic of multiplicities in production and decay in  $b\bar{b}$  event. (b) Definition of impact parameter.
11. Distribution of impact parameter  $\delta$ , b-enriched and b-depleted distributions compared, from TASSO<sup>33</sup>.
12.  $\delta$ -distribution of selected (a) muons (b) electrons: JADE. Dashed lines are Gaussian fits of zero mean. Full lines use  $\tau(b) = 1.8$  ps.
13. Best projected decay length distribution (TASSO). Data-points with errors. Histogram - best MC fit.
14. Dipole moment method (a) jet axis and track production vertices (b) production points of tracks in each jet (c) average vertex for each jet and dipole moment.
15. Dipole moment distribution (TASSO). Data compared to Monte Carlo for  $\tau(b) = 1.4$  and 0 ps.
16. (a)  $e^+e^-$  event at  $W = 44$  GeV (TASSO) (b) vertex region greatly magnified. Cross marks beam spot centre. Sum of weights in upper jet  $\Sigma W = 4.33$  and in lower jet  $\Sigma W = 7.88$ .
17. Jet charged multiplicity distributions (TASSO). Comparison of jet recoiling against b-tag jet and average jet at  $W = 42.1$  GeV (a) raw data (b) after correction for detector acceptance.

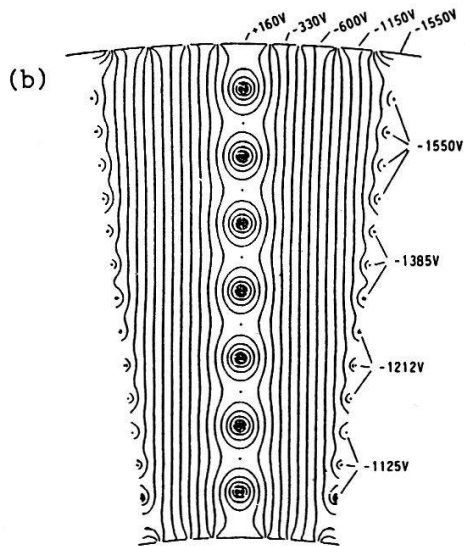
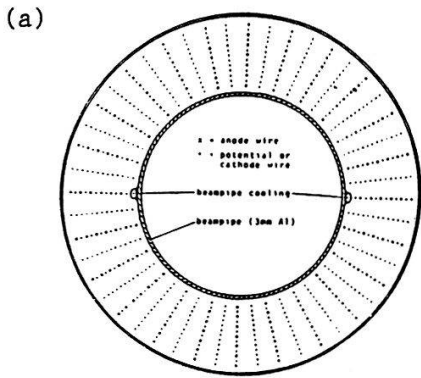


Fig 1

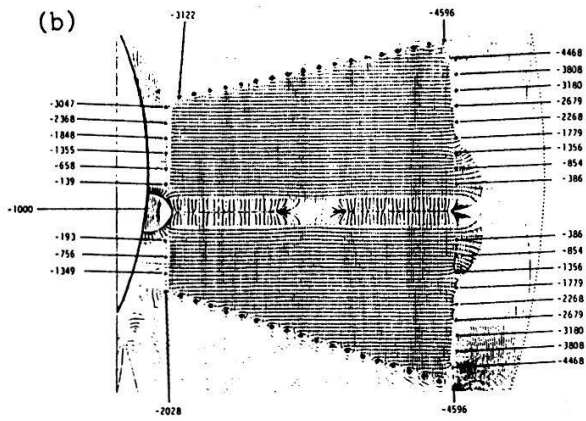
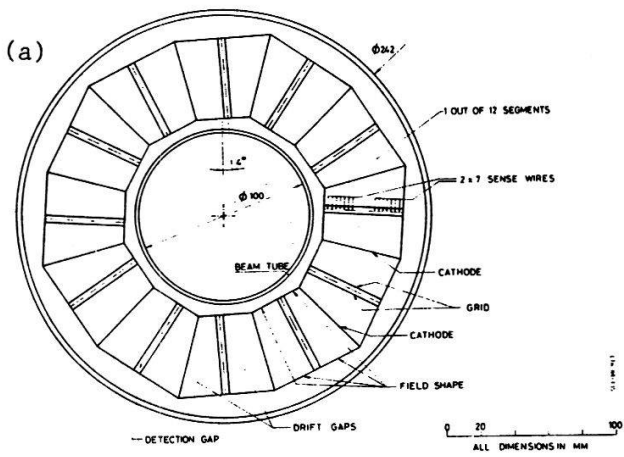


Fig 2

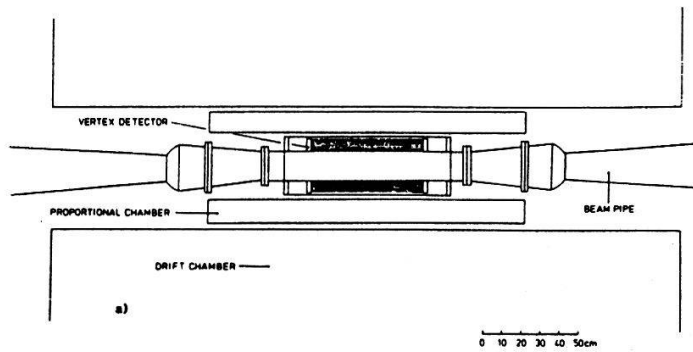
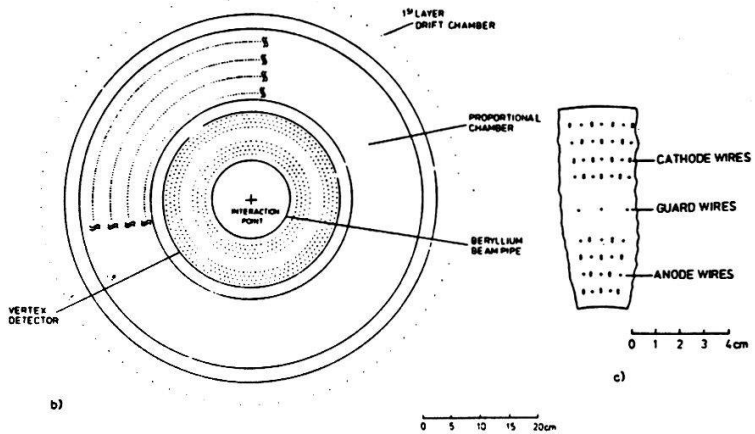


Fig 3



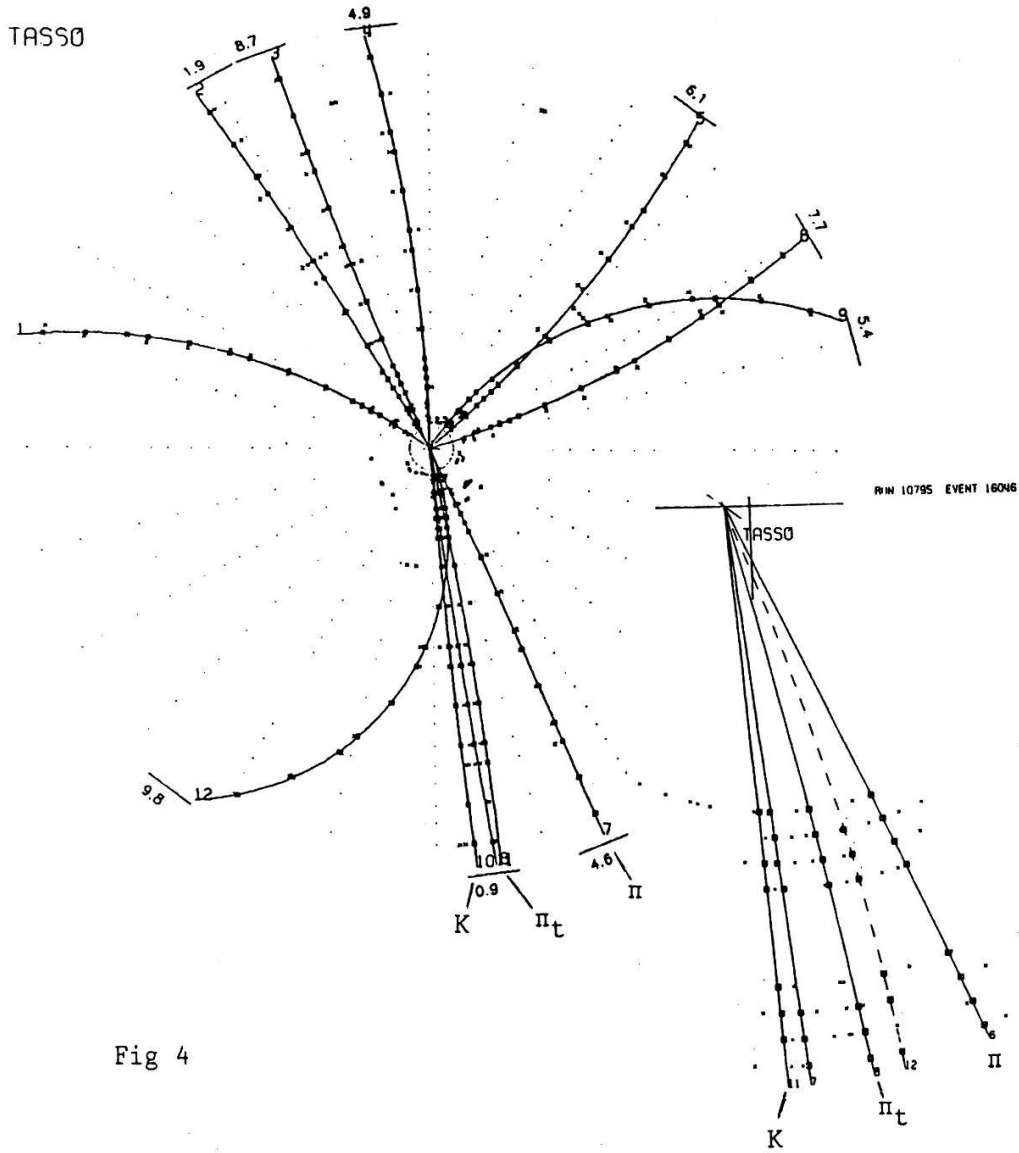


Fig 4

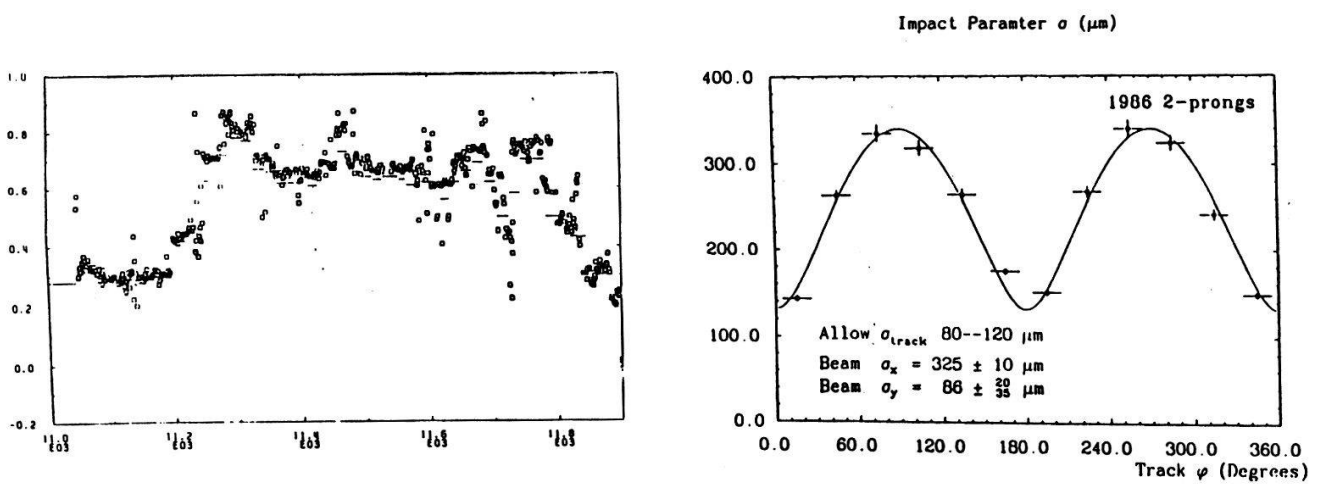


Fig 5

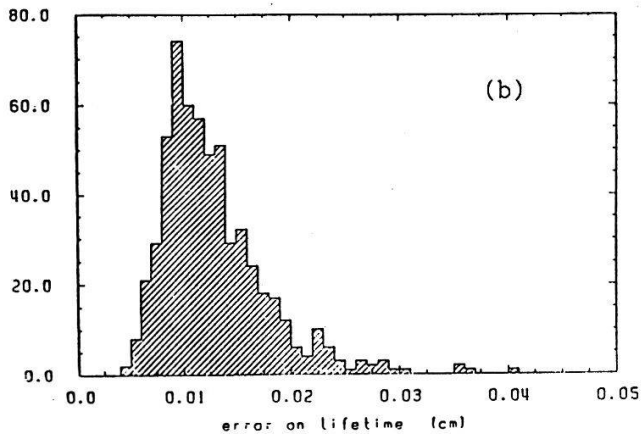
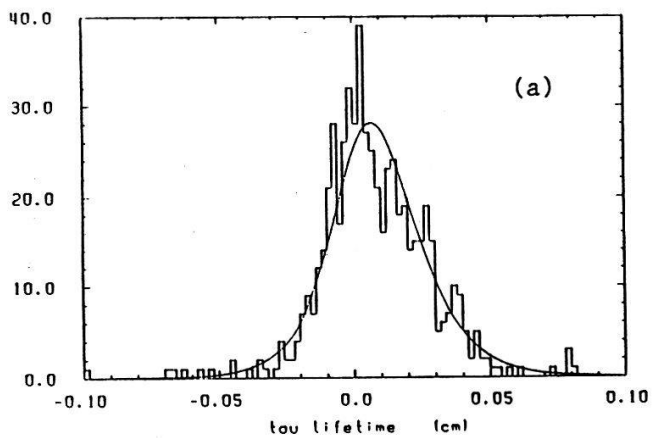


Fig 6

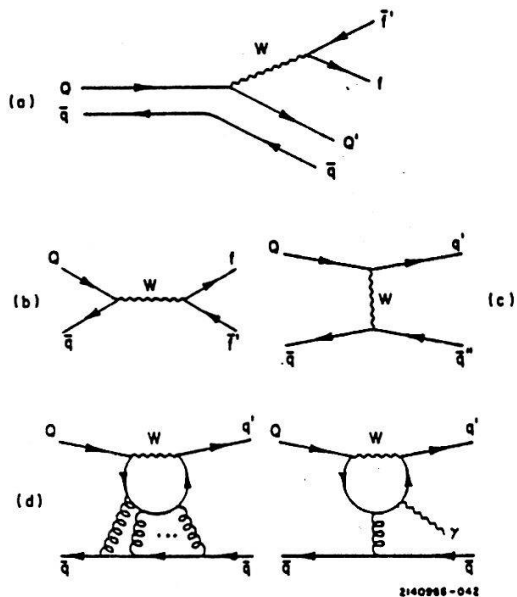


Fig 7

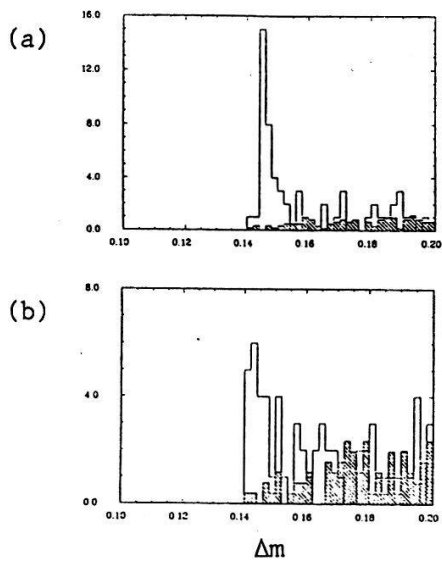
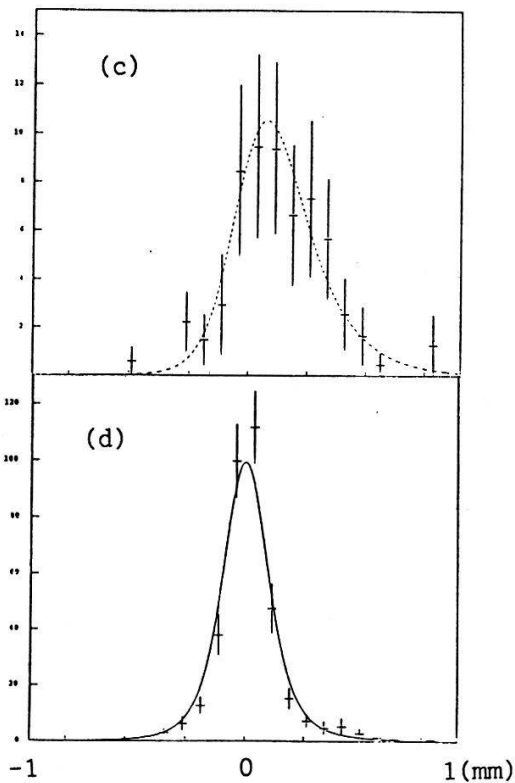


Fig 8



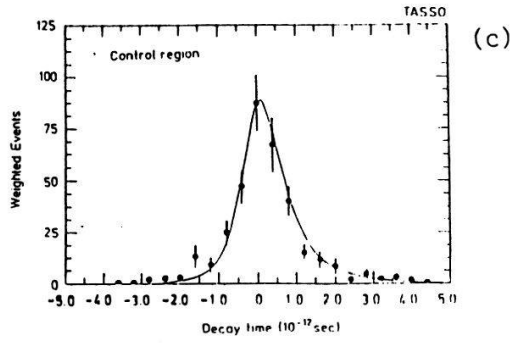
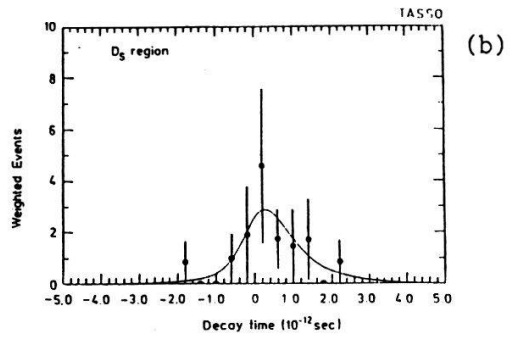
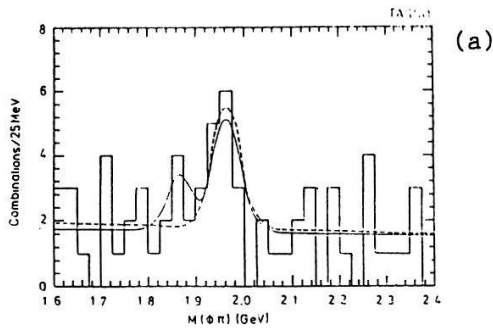


Fig 9

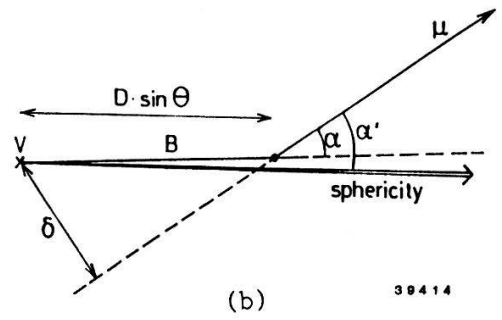
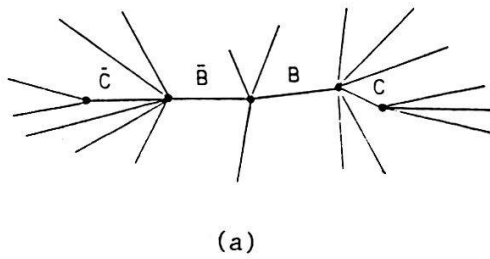


Fig 10

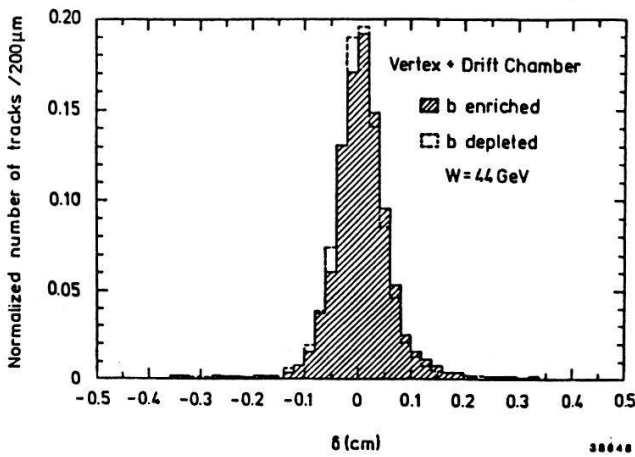


Fig 11

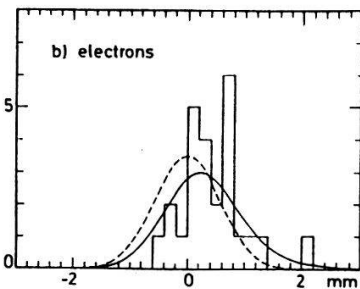
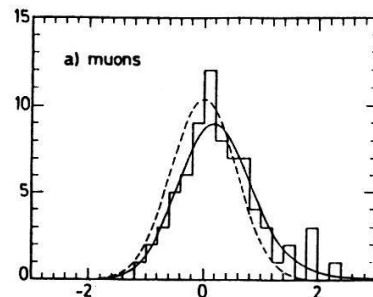


Fig 12

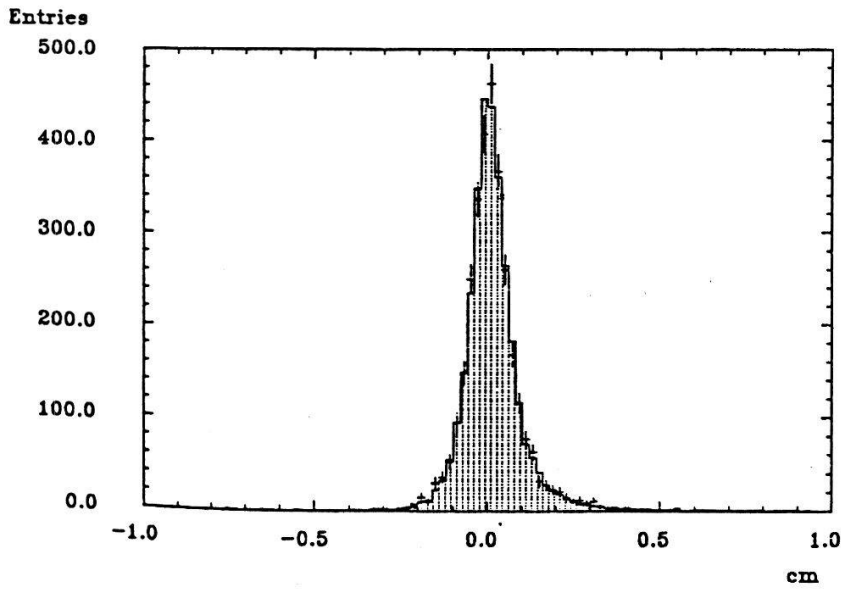


Fig 13

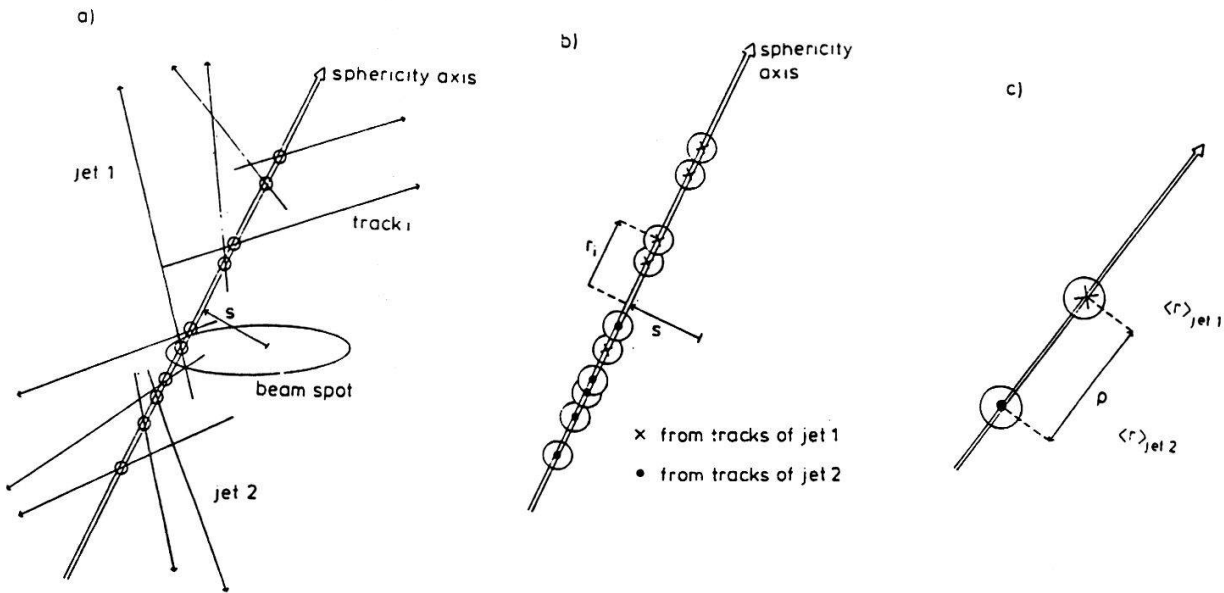


Fig 14

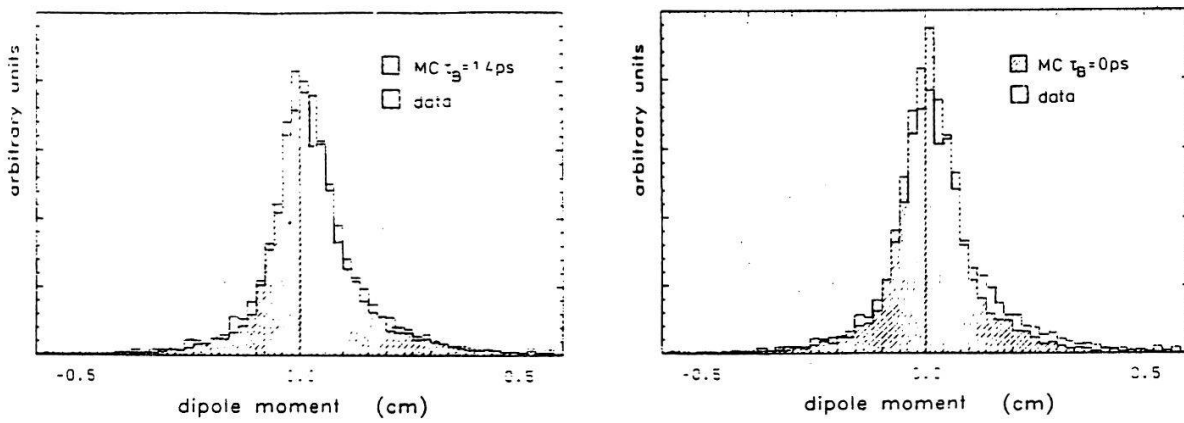
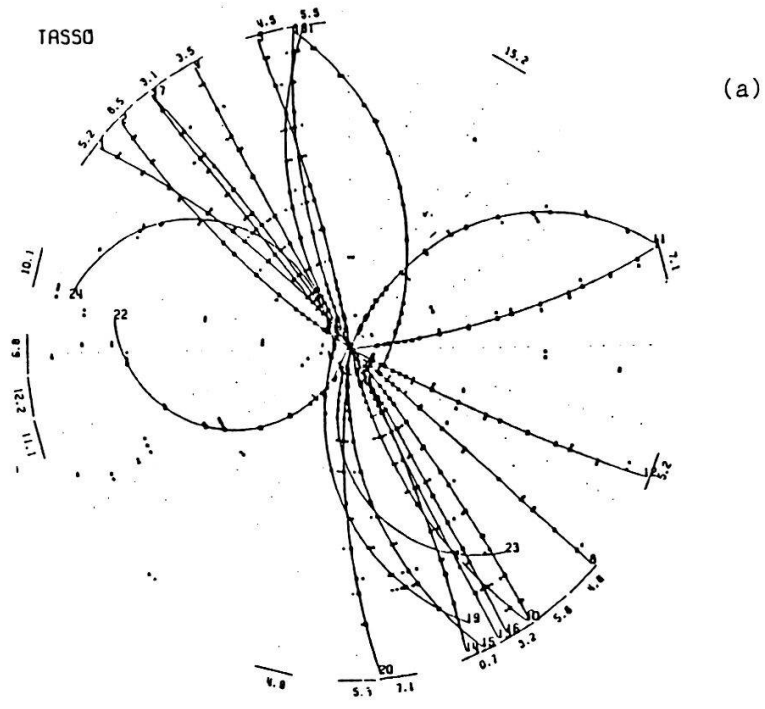


Fig 15



(a)

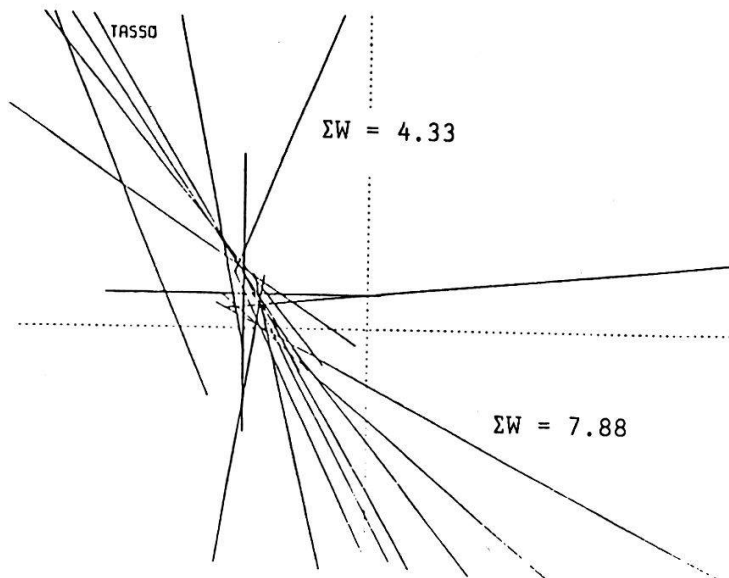


Fig 16

(b)

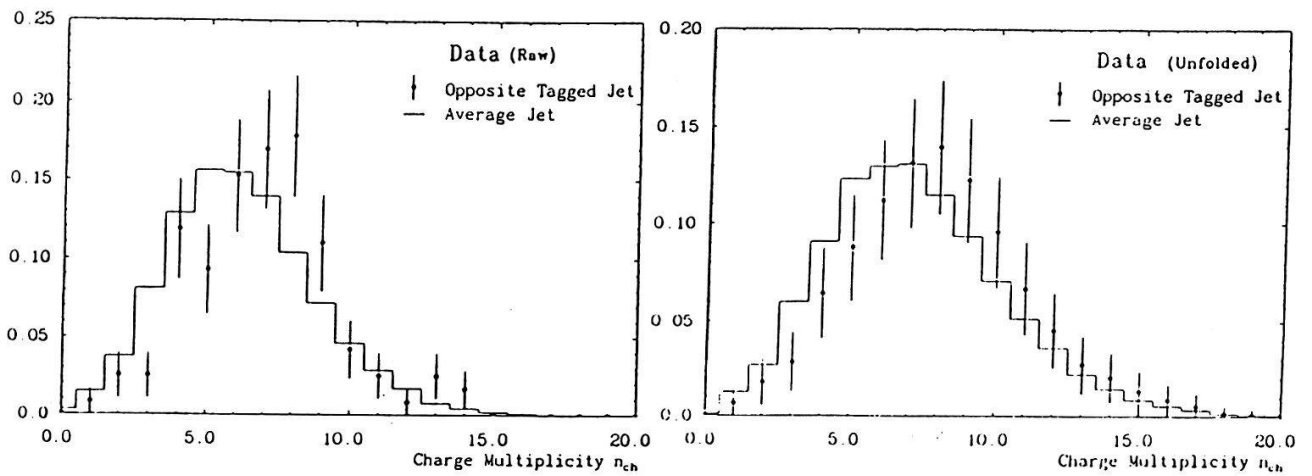


Fig 17